Molecular Catalysis 528 (2022) 112511

Contents lists available at ScienceDirect

Molecular Catalysis

journal homepage: www.journals.elsevier.com/molecular-catalysis

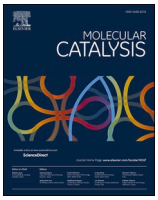

Synthesis of heterocycles compounds from condensation of limonene with aldehydes using heteropolyacids supported on metal oxides

Julián E. Sánchez-Velandia [a,*], Herme G. Baldoví [b], A. Yu Sidorenko [c], Jaime A. Becerra [d], Fernando Martínez O [a,*]

[a] Centro de Investigaciones en Catálisis-CICAT, Universidad Industrial de Santander Escuela de Química, Km 2 vía El Refugio, Piedecuesta, Santander, Colombia
[b] Departamento de Química, Universidad Politécnica de Valencia, Camino de Vera s/n, 46022, Spain
[c] Institute of Chemistry of New Materials of National Academy of Sciences of Belarus, Skaryna str, 36, Minsk 220141, Belarus
[d] Environmental Catalysis Research Group, Chemical Engineering Department, Engineering Faculty, Universidad de Antioquia UdeA, Calle 70 No. 52-21, Medellín, Colombia

A B S T R A C T

In this contribution, heterogeneous materials based on heteropolyacids (HPA, $H_3PW_{12}0_{40}$ hydrate) supported over several metal oxides (TiO_2, SiO_2, SBA-15, Al_2O_3) were prepared using wetness impregnation, characterized by XRD, FTIR, SEM, acidity by TPD, nitrogen physisorption, RAMAN spectroscopy, ^{31}P NMR and then evaluated in the catalytic condensation of limonene with benzaldehyde. After incorporation of HPA over each support, no structural changes were observed as it was suggest by FTIR, RAMAN and XRD. Acidity analysis by TPD-NH_3 showed that increasing the HPA amount increases the acidity of the catalyst until it is constant (20–30%). HPA over alumina, silica and SBA-15 also showed high values of acidity but less than typical HPA/P25 catalyst (HPA over commercial Degussa P25). This last was one of the most selective materials (surface area of 39 m^2/g and acidity of 187 μmol NH_3. g_{cat}^{-1}) for the synthesis of 3-oxabyciclo[3.3.1]nonane (up to 80%) with a low selectivity to the limonene isomers by-products. The use of water as a solvent decreased considerably the catalytic activity. The same observation was found when the volume of the solvent increased to 30 mL. Besides, catalytic condensation can be performed at free solvent conditions and at room temperature; however, when decrease temperature, a higher number of isomers was observed rather than the desired product. In addition, catalytic condensation was also evaluated in biomass of essential oils and mixtures with sesquiterpenes showing good to excellent results. Typical LHHW mechanism was evident after kinetic analysis. HPA/P25 was shown to be a robust material since can be reused up to two times with a possible decrease in its catalytic activity.

1. Introduction

The molecules containing agro-industrial wastes can be used as an alternative sources for the production of chemicals like fragrances, food additives, biofuel, vitamins, antioxidants, etc. [1]. Chemical molecules from biomass are structurally different from the carbon forms in fossil resources and then, their transformation into valuable products is a current challenge. Monoterpenes are molecules considered as an important and valuable start platforms of chemicals that can be converted into a lot of substances with potential and attractive attention in the fine chemistry industry (pharmaceutical, medical, agrochemical, etc.) [2,3]. In addition, these compounds and their derivatives play an important role in the creation of new biologically active substances [4].

The transformation of monoterpenes and monoterpenoids has been addressed using different chemical routes, including isomerization [5,6], biotransformation [7], condensation [8] oxo-transfer [9], alkylation [10], hydrolysis [11], pyrolysis [12], among other. Condensation of terpene compounds with aldehydes makes it possible to obtain heterocyclic products with various types of structures like chromene [13,14], isobenzofuran [4,15], as well as complex polycyclic molecules [16]. It is known that some of these products exhibit high biological activity (analgesic, antiviral, antitumor), and can also be used in fine chemistry and perfumery [17,18]. Thus, 3-oxabicyclo[3.3.1]nonane compounds or their derivatives are one type of molecules that can be obtained through condensation of monoterpenes with aldehydes. The excellent properties as a biological precursor, as well as metabolites (or as fragrance), reinforce their importance to be investigated [19]. Even, these compounds are important synthons that offer an important platform for the construction of biologically/medicinally substances with numerous stereocenters [20]. It should be noted that some of the molecules with a 3-oxabicyclo[3.3.1]nonane structure are potent inhibitors of the TDP1 enzyme, a target for anticancer therapy [15]. Heterogeneous catalysts can be used as greener, sustainable, and more efficient routes for the synthesis of oxabicyclic or isobenzofuranes-like compounds. There are a lot of advantages for using heterogeneous materials for the transformation of chemicals into high-added value substances

* Corresponding authors.
E-mail addresses: julian.sanchezv@udea.edu.co (J.E. Sánchez-Velandia), fmartine@uis.edu.co (F. Martínez O).

https://doi.org/10.1016/j.mcat.2022.112511
Received 1 June 2022; Received in revised form 9 July 2022; Accepted 12 July 2022
Available online 18 July 2022

including economic impact and robustness (among others) which could improve many of the current processes. Then, the use of heterogeneous catalysts is an efficient alternative for the synthesis of isobenzofurans-like compounds.

It has been reported that isobenzofurans derivatives, with a pharmaceutical potential, can be achieved from renewable 2-carene over halloysite nanotubes (Fig. 1a) [21]. The highest selectivity to the desired target (ca. 70%, at soft reaction conditions: 50 °C, 1.0 g of catalyst, 0.1 g of monoterpene, 0.1 of anisaldehyde) was related to the weak Brønsted acid sites, which promote the condensation rather than parallel isomerization (side reaction). Similarly, heteropoly acid catalysts (and its acidic Cs salt: $Cs_{2.5}H_{0.5}PW_{12}O_{40}$) were tested for the synthesis of 3-oxabicyclo[3.3.1]nonane (Fig. 1b) with a wide class of monoterpenes (including α-pinene, β-pinene, limonene, nerol, α-terpineol) and benzaldehyde, cuminaldehyde and *trans*-cinnamaldehyde [8]. High yields were observed at relatively benign conditions (dimethyl carbonate or 2-methyltetrahydrofuran and 50 °C). However, it is seeming dubious that the synthesis of these kinds of compounds from bicycle α- and β-pinene is because of their strainer internal structure which must favor the isomerization instead of condensation. In this case, the monovalent cation of Keggin's structure, $Cs_{2.5}H_{0.5}PW_{12}O_{40}$, was applied because of its strong Brønsted acidity, larger surface and high thermal stability. Taking this into account, condensation of bicycle monoterpenes (such as 3-carene and pinenes) with aromatic aldehydes should be favored with weak Brønsted acid sites while condensation of cyclic monoterpenes (such as limonene) is stand up for strong Brønsted acid sites. Then, Brønsted acid sites should be considered for these types of C-C condensation reactions as an important parameter to be studied.

Heteropolyacids catalysts (HPA) with a typical Keggin's structure have been applied for numerous reactions: esterification and biomass conversion [22], selective sulfoxidation [23], methacrolein oxidation [24], among others, and their excellent features as heterogeneous catalysts is because their acidity which allows obtaining selectively different targets. Its Brønsted acidity is due to the ionic structure which permits high proton mobility. However, their main disadvantage is related to their easy lixiviation in polar solvents. It is for this reason that dispersion/anchoring/impregnation of this type of HPA on inert supported materials should enhance their robustness and then, their recyclability in catalytic reactions. Also, increasing their thermal stability and improving acid strength in inert solids [25]. Among of the supports, metal oxides have shown to be interesting because of their high surface area, good mechanical stability, and besides they are biocompatible. For example, titanium dioxide is a material of choice in several applications which include cell attachment and proliferation [26]. Together with HPA could be applied in both pharmaceutical and medical industries. Considering the advantages of titanium dioxide together with the use of heteropolyacids for increasing the acidity and for using in condensation reactions, these kinds of materials could be an alternative strategy to propose rather than previous heterogeneous HPA/SiO_2 [8]. In addition, and considering the lack of metal oxides used for the condensation of limonene with benzaldehyde, other supports based on metal oxides could be also tested.

Prompted by the properties and acidity of heteropolyacids catalysts, in this contribution, we have evaluated the catalytic activity of the HPA supported on inert oxides such as titanium oxide, silica nanoparticles and SBA-15 in the selectivity synthesis of 3-oxabyciclo[3.3.1]nonane like compounds from the condensation of limonene and benzaldehyde. The parameters evaluated were the amount of HPA impregnated on the best support, amount of aldehyde, temperature, and nature of acid support. Limonene was chosen because of its availability and besides that is a large-tonnage waste juice production [27,28]. The relationship between surface textural properties and acidity was elucidated. Finally, kinetics was also included in this research incorporating the parameters of both pseudo-homogeneous and heterogeneous models fitted to experimental tests by using a genetic algorithm. For the best of our knowledge, no detailed study on this topic has been regarding until now.

2. Methodology

2.1. Synthesis of HPA impregnated on inert oxides

Heteropolyacid ($H_3PW_{12}0_{40}$ hydrate from Aldrich) supported on inert oxides (TiO_2-P25 from Sigma Aldrich (S_{BET} = 34 m^2 g^{-1}) SBA-15, titanium nanopowder from Sigma-Aldrich (S_{BET} = 45 m^2 g^{-1}), Alumina (S_{BET} = 40 m^2g^{-1}), silica (S_{BET} = 28 m^2 g^{-1}) were prepared by wetness impregnation. Briefly, 0.12 g of HPA (20 wt%) was dispersed on 0.6 of each support (previously dried at 110 °C for 2 h) and then, 30 mL of water was added. The mixture was constantly stirred for 2 h and afterward dried at 110 °C for 17 h. Finally, the solid was calcined at 300 °C for 5 h (2 °C min^{-1} under static air). At this temperature, Keggin's structure is maintained to assure the impregnation of HPA on the support. The solids were named HPA/S, where HPA stands for heteropolyacids while S means support (used during each impregnation).

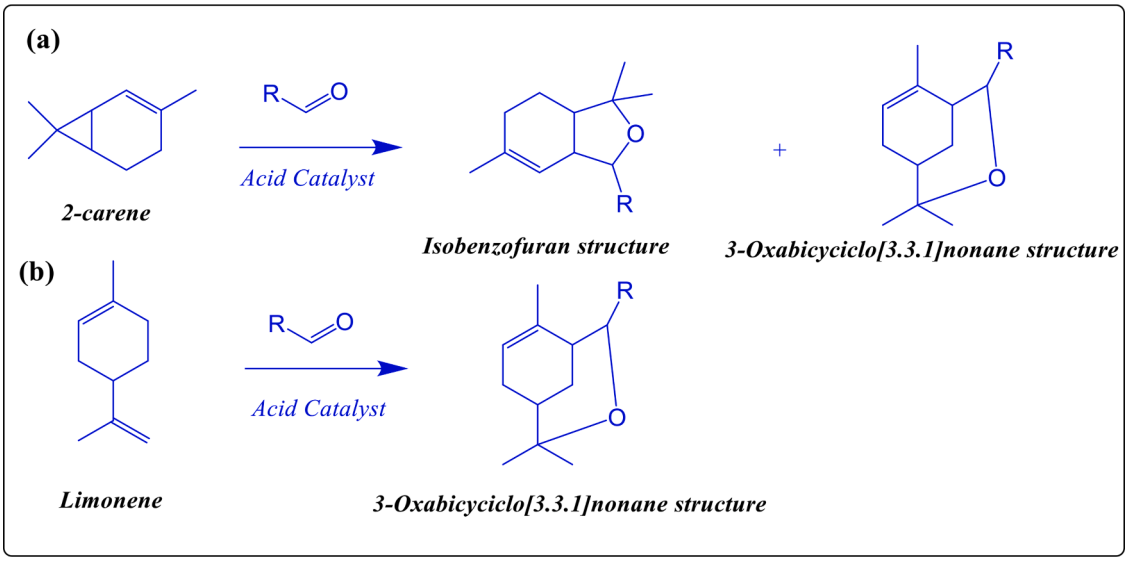

Fig. 1. (a) Isobenzofurane derivative (b) 3-oxabicyclo [3.3.1] nonane, products of the condensation of monoterpenes with aldehydes. R means aromatic derived aldehyde.

2.2. Characterization techniques

X-ray powder diffraction (XRD) data were measured with a Bruker PANalytical Empyrean diffractometer (Malvern Instruments Limited, Malvern, UK) (Cu Kα radiation) in transmission geometry. The analysis by FTIR was performed in a Perkin Elmer Frontier spectrum 65 model with a resolution of 4 cm^{-1} and 64 scans. The morphology and the composition of each material were characterized using a high-resolution field emission scanning electron microscope (HRFESEM from Zeiss instruments, Model GeminiSEM 500), equipped with Energy dispersive X-ray detector, EDS (OXFORD INSTRUMENTS) for composition analysis. Nitrogen adsorption/desorption isotherms at 77 K were measured on a Micromeritics Tristar 3000 apparatus at -196 °C. Before analysis, the samples were degassed under vacuum at 150 °C for 12 h. The specific surface area was determined from the linear part (0 - 0.23 P/P_0) of the BET plot. The total pore volume was measured from the isotherms at $P/P_0 = 0.95$ and the mean pore diameter was determined by the BJH method applied to the adsorption branch. Raman spectra were collected with a Renishaw In Via "Reflex" Raman Spectrometer equipped with an Olympus microscope and a CCD Detector using a 325 nm laser with a power of 15 mW as the excitation source. The spectra were collected by averaging 10 scans at a resolution of 3 cm^{-1}. The acidity of the catalysts was determined by temperature-programmed pulsed adsorption and desorption of ammonia (NH_3-TPD) experiments utilizing a Micromeritrics Autochem II paired with an OmniStar Balzers Instrument mass chromatograph. The sample amount of 0.95 g was prepared to remove any adsorbed solvent, water or gas adsorbed, by pre-treating it (in vacuum) with Ar flow of 10 mL/min at 200 ºC for 1 h and a He flow of 10 mL/min at 200 ºC for 20 min. Then, analysis of the samples was performed after cooling down to room temperature starting with a pulsed adsorption of ammonia with a He flow of 100 mL min^{-1} at 100 ºC. Each pulse of ammonia lasted 10 min and NH_3 was introduced to the system via a 0.5 mL loop at 100 ºC. When the sample was saturated with NH_3, the desorption process started with a He flow of 100 mL/min and heating up to 500 ºC for 5 min (heating rate of 10 ºC min^{-1}). gasses desorbed were monitored by online QMS (Quadrupole Mass Spectroscopy) analysis. The total acidity of the catalyst was calculated by integration of the NH_3 desorption profile referred to as the QM signal, at mass 15. Such mass value was preferred to the mass signal at 17, to exclude any contribution due to water fragmentation. Thermogravimetric analyses were performed on a TGA/SDTA851e METTLER TOLEDO station. Analysis was carried out under O_2 atmosphere and heated up to 900 ºC (rate of 10 ºC min^{-1})

2.3. Catalytic reactions

Initial catalytic tests were carried out with limonene and benzaldehyde (purchased from Sigma-Aldrich with a purity of at least 98%) and they were used as received at least otherwise. Catalytic reactions were performed in 15 mL batch reactors under magnetic stirring. In a typical experiment, the selected amount of catalyst (10, 20, 30 mg) was added to different amounts of limonene and benzaldehyde (Typically 1 mmol and 3 mmol, respectively) and constantly stirred for 5 h and 50 °C. Catalysts were ground for obtaining a particle size of <100 μm and the final mixture was stirred at 750 rpm, with the objective to ensure no diffusional problems related to internal and external mass transfer. The products were identified by gas chromatography with a mass selective (GC–MS) and FID, Agilent 6890, and HP-1 column (100 m x 250 μm x 0.5 μm). The carrier gas was N_2 (23.80 mL min^{-1}) and the split ratio was 15:1. The oven temperature was kept at 50 °C for 3 min and then it was raised to 180 °C at 15 °C min^{-1} and maintained at that temperature for 2 min. Finally, the oven temperature was again raised to 300 °C at 15 °C and maintained for 2 min. *n*-Heptane was used as an internal standard. Balance of mass was verified checking that it was at around 100% (95–100%). Reactions with essential oils were carried out in the same way. Turpentine oil (72% α-pinene, 9% β-pinene, 1% camphene, 2% limonene, 16% others) was acquired from MultiQuímicos (Bucaramanga, Colombia) while *Rosmarinus* oil (19% α-pinene, 11% β-pinene, 7% camphene, 16% limonene, 2% *p*-cymene, 45% others) was purchased from Perfumes&Aromas (Colombia). The corresponding 3-oxabyciclo[3.3.1]nonane was isolated and purified from the reaction mixture using preparative thin layer chromatography with petroleum ether and ethyl acetate as eluent solvents. The product was well identified using NMR (^1H and ^{13}C) (reported previously in [29] and which correspond to 3-oxabyciclo[3.3.1]nonane; supporting information)

2.4. Kinetic assessments

For the kinetic analysis of the condensation of limonene with benzaldehyde, reaction rates were calculated by the initial reaction rate method from experimental data of concentration in a liquid-phase batch reactor at several conditions shown in Table 1. The details of the calculations of the reaction rate by initial reaction rate method is presented in Supporting Information. The kinetic parameters were obtained through an optimization of the sum of squared errors in an objective function fitting experimental reaction rate calculations with some kinetics expressions incorporating the Genetic Algorithm (GA) in Matlab software. The GA is a method for solving constrained and unconstrained optimization problems (with discontinuous, nondifferentiable, stochastics or highly nonlinear objective functions) based on natural selection, randomly modifying a population of individual solutions. The proposed kinetics expressions stablished from heterogeneous models based on the Langmuir-Hinshelwood-Hougen-Watson (LHHW) and Eley-Rideal (ER) mechanisms, along with a power law based pseudo-homogeneous (pH) model.

3. Results and discussion

3.1. Catalyst characterization

3.1.1. FTIR measurements

Fig. S1 (in Supporting Information) shows the IR spectrum for all HPA synthetized and impregnated catalysts in comparison with the HPA ($H_3PW_{12}O_{40}$ hydrate) pattern. The spectrum of the HPA pattern clearly shows the characteristic bands of the $[PW_{12}O_{40}]^{3-}$ Keggin anion at 1080 (υ_{as}(P-O_a)), 982 (υ_{as} (W-Od)), 890 (υ_{as} (W-Ob-W)), and 800 cm^{-1} (υ_{as}(W-Oc-W)) [30]. It seems that in all supported catalysts, no bands related to the typical vibration of Keggin anion were observed which could be associated with a homogeneous dispersion of this polyoxometalate acid in all supports or because of the H-bonding interactions with the supports which could be disturbed by dipole-dipole interactions [31]. On the contrary, typical vibrations of each support were noticed. For example, for SBA-15 material, bands at around 960 and 1090 cm^{-1} corresponding to Si-OH vibration and Si-O-Si asymmetric stretching vibration of SiO_2 were observed [32]. In the case of HPA/SBA-15, the same bands that parent SBA-15 were found. In addition, for HPA supported on silica nanoparticles HPA/np-SiO_2 the same vibrations were achieved. For titanium dioxide patterns and their modification with HPA (that includes titanium dioxide HPA/P25 and

Table 1
Set of experiments and reaction conditions used for the kinetic analysis.

Test set	n_A/n_B	m_A (g)	$m_{catalyst}$ (g)	V (mL)
1	7.3873	0.0658	0.0310	0.4515
2	2.4298	0.2000	0.0306	0.6110
3	3.6230	0.1331	0.0305	0.5286
4	2.9883	0.2659	0.0301	0.9264
5	8.6758	0.0134	0.0305	0.1052

ni: mol of specie i (A: limonene, B: benzaldehyde), all tests with HPA/P-25, V: volume of the reaction. Each set test comprises 7 individual experiments at different times of reaction: 5, 15, 30, 45-, 60-, 120-, and 300-min. Conditions: 750 rpm, 50 °C.

nano powder HPA/NP-TiO_2) show bands at 500 and 600 cm^{-1}due to typical Ti-O and Ti-O-Ti vibrations [33]. For both Al_2O_3 and HPA/Al_2O_3, it seems the typical Al-O stretching band in octahedral structure at 459, 595 and 656 cm^{-1}. On the other hand, Al-O and Al-O-H bands at 715 and 1072 $cm^{-1}$are related to symmetrical bending mode. In addition, the broad peak between 900 and 1100 cm^{-1} are assigned to O-H deformation vibrations [34].

3.1.2. X-ray diffraction

To obtain information about the crystallographic structure of each material, XRD patterns are shown in Fig. 2. In the case of the homogeneous Keggin's acid, it shows the typical shifts which are assigned to $H_3PW_{12}O_{40}{\cdot}14H_2O$ according to JCPDS data [35]. It is well known that Keggin anion in the heteropolyacid structure is composed of a central PO_4 tetrahedron unit surrounded by 12 edge- and corner- sharing metal-oxygen octahedral WO_6. Secondary structures are formed by protonated species of water (e.g., $H_5O_2^+$) which connect four heteropoly anions using a hydrogen bond with the terminal M=O atoms (M is metal and O is oxygen). When heteropolyacid was impregnated on different metal oxides, the typical signals attributed to the HPA disappeared while the shifts of each support appear slightly. For example, the well-defined peaks for HPA/SiO_2 show the signals of the SiO_2 together with the typical heteropolyacid shifts. Similarly, for both HPA supported on titanium dioxide nanopowder and P25 showed the anatase and rutile phases in all the ranges at the shifts: 25.4°, 38.0°, 48.0° and 54.7° (JCDPS No. 21-1272) [36,37]. For the material modified over alumina, the typical γ-phase of alumina appears with the (3 1 1), (2 2 2), (4 0 0) and (4 4 0) reflections [38,39]. In general, there were no intense peaks corresponding to the crystalline structure of the HPA phase detected for all the catalysts. This clearly indicates that HPA could be highly dispersed on the support of amorphous WO_x species (Because of the calcination time) which were decomposed during the synthesis.

3.1.3. Textural properties

Table 2 shows the textural properties measured for all heterogeneous HPA catalysts. It is seeming that the surface area for HPA homogeneous (5 $m^2\ g^{-1}$) is lower in comparison to other materials. It has been reported the low surface area of non-supported Kegging's structure [40,41]; however, changes are observed when different supports are impregnated within heteropolyacids. For example, when P25 (titanium dioxide from Degussa P25, composed mainly for Anatase) is used as support a decrease in the surface area is observed when different amounts of HPA are incorporated. Although these differences are not significant, it is observed a decrease in the surface area could be attributed to the block of the pores or the formation of small crystal (or aggregates) that appears to change structurally the catalyst structure [41]. On the other hand, different charges of HPA over P25 do not affect the surface area of the material. This fact could be associated with the same crystal size which is directly related to the surface area of the material [42]. Besides, when preparation of the catalyst was scaled up to 10 g, it was found that the surface area is almost the same (34 $m^2\ g^{-1}$) allowing to verify the high reproducibility of the synthesis of the material.

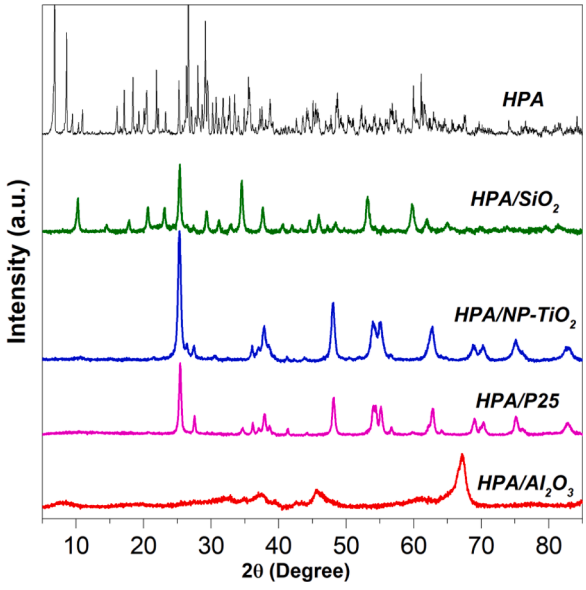

Fig. 2. XRD pattern of HPA supported on several oxides.

Table 2
Textural properties for the synthetized HPA supported catalysts.

Catalyst	S_{BET} ($m^2\ g^{-1}$)	S_{meso} ($m^2\ g^{-1}$)	Pore volume ($cm^3\ g^{-1}$)	Dp (nm)
HPA	3	-	-	-
HPA/SiO_2	19	-	0.10	9
P25	49	-	-	-
5-HPA/P25	37	-	-	-
10-HPA/P25	36	-	-	-
20-HPA/P25	39	-	-	-
NP-TiO_2	73	20	0.25	13
HPA/NP-TiO_2	62	9	0.13	10
SBA-15	555	481	0.40	25
HPA/SBA-15	444	386	0.23	7.2
Al_2O_3	129	100	0.60	12
HPA/Al_2O_3	81	77	0.41	9.1

Comparatively, when titanium dioxide nano powder, NP-TiO_2, was used as support, the surface also decreased after incorporation of the HPA unit, but its surface area is higher, again, with respect to typical Degussa P25. On the other hand, other materials with different geometries and structures were also used: SBA-15 and γ-alumina. Similarly, when HPA is impregnated over both supports, the surface area decreases significantly up to 444 and 81 $m^2\ g^{-1}$, respectively. In the case of SBA-15 materials, the apparent mesoporous surface area is drastically affected by the incorporation of kegging's unit. In general, changes in surface area in all supports are affected with a minimum of 15% and a maximum of 37% with respect to the support without modification.

3.1.4. Scanning electronic microscopy (SEM)

Some selected HPA supported on P25, SBA-15 and SiO_2 are showed in Fig. 3. For HPA/P25 (Fig. 3 (a, b)), it seems a large distribution of boundary rugosity together with small particles on the surface. Some cylindrical geometries with irregular shape together with jagged edges were also observed. In the case of HPA/SBA-15 (Fig. 3 (c, d)) several ropes like shape particles were seen and it appears that the size of the ropes is relatively uniform. On the other hand, these thin ropes can be aggregates making macroscopic structure with a well wheat like structure defined. Similar observations have been reported previously [43]. For HPA/SiO_2, among of the particles observed were of similar shape and even of size that such obtained for HPA/SBA-15 (Fig. 3 (e, f)). White spots over the surface of silicon oxide are observed with a good dispersion. These particles are mainly associated with the deposition of heteropolyacid over the typical structure of the material.

3.1.5. Raman spectroscopy

Typical Raman spectra were acquired for almost all the samples, and they are showed in Fig. S2 (Supporting information). In the case of HPA/P25 it seems typical bands of the rutile phase at 448 cm^{-1} and at 610 cm^{-1} which are characteristics of the E_g and A_{1g} vibrational modes [44]. The same bands and behavior were observed for HPA supported on titanium dioxide nanotubes. Interestingly, for both samples no band at 1010 cm^{-1} was observed (characteristic for the Keggin structure) [45]. Contrary, this band was detected for both HPA/Al_2O_3 and HPA/SiO_2 materials showing a slight dispersion of the heteropolyacid on each

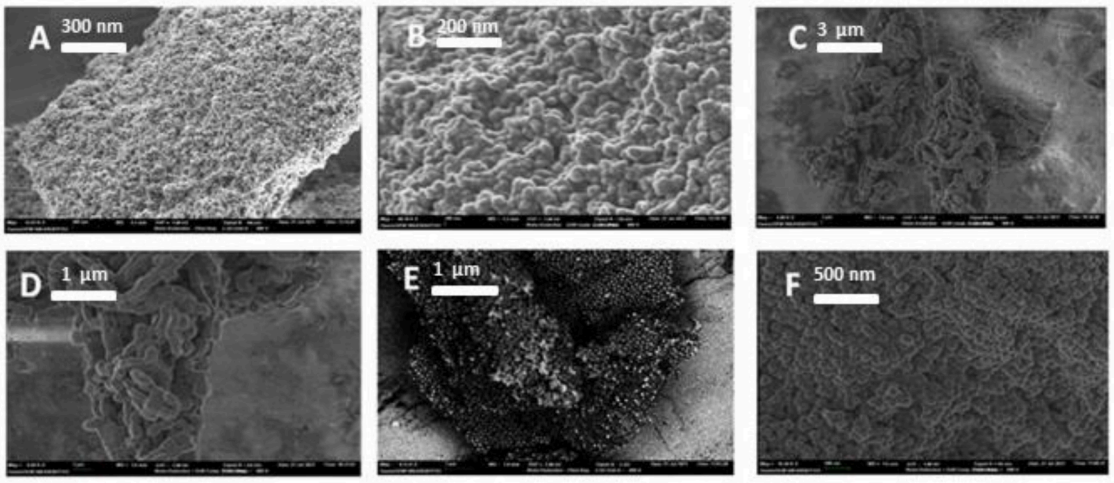

Fig. 3. SEM images of: (A, B) HPA/P25 (C, D) HPA/SBA-15 (E, F) HPA/NP-SiO_2.

support. A broad peak at around 930–950 cm^{-1} could be attributed to B_u mode of γ-Al_2O_3 [46]. For HPA/SBA-15 and HPA/SiO_2 a band at 1600 cm^{-1} is associated to typical vibration of Si-O-Si which is in line with the observations achieved by using FTIR (Section 3.1.1).

3.1.6. NMR measurements

Solid-state nuclear magnetic resonance spectroscopy is an atomic-level method to determine the chemical structure among contain atoms such as phosphorus, aluminum, etc. [47]. Analysis of solid-state of ^{31}P NMR spectrum can indicates a chemical interaction of PW unit with the support. In the literature it is well reported two kinds of peaks when HPA is supported on different oxides: a peak at around -15 ppm related with intact Keggin structure and another in -14 ppm associated with species such as $H_6P_2W_{18}O_{62}$ or $H_6P_2W_{21}O_{71}$ [48]. Also, because of the standard (H_3PO_4 in many of the cases), this shift can be improved at least 0.01 ppm, making better the process of identification of the species [49]. Fig. S3 (in supporting information) shows the ^{31}P NMR spectrum for the homogeneous heteropolyacids (H_3PWO_{40}) and for HPA supported on SBA-15, SiO_2 and titanium dioxide Degussa P25. In all samples, a wide signal at around -15.4 ppm is observed evidencing the presence of the Keggin structure after its incorporation over the support or also the presence of several coexisting species such as α- $[PW_{12}O_{4O}]^{3-}$ [49]. Apparently after incorporation of the monolayer of heteropolyacids over each support, the characteristic peak which suggest the presence of the fundamental unit of the heteropolyacids is not shifted, however, in the case of HPA/P25 it seems a broad band close to the region of -10 to -5 ppm. This band (peak) is mainly associated with structural changes of Keggin unit and possible defects in the molecule which are not possible to detect because of the conditions of the experiment. Considering these results and the previous one based on FTIR and XRD, it could be possible to suggest that possibly heteropolyacids is dispersed in each support as its fundamental cations rather than the typical crystal structure.

3.1.7. Temperature programmed desorption of ammonia (TPDA)

Catalyst acidity is an important feature to be considered, being a variable that can be measured by different ways; one of them is the desorption of ammonia at different temperatures. This is a procedure that indicates the strength and the amount of acid sites in a material. The values of total acidity are showed in Table 3. As can be seen, the catalyst with the highest content of acidity (up to 214 µmol g_{cat}^{-1}) was the HPA/NP-TiO_2, while the HPA/P25 with both 20% and 30% wt had similar values of acidity. Interestingly, the variation of the amount of heteropolyacid on titanium dioxide increases its acidity (5–20%), however, at high loading of HPA (25%, 30%) the total acidity appears to keep constant (183–187 µmol/g-cat). In fact, the increases of heteropolyacid increases the acidity of typical titanium dioxide.

Table 3
Acidity for different heteropolyacids supported materials.

Material	Total acidity (µmol g_{cat}^{-1})
HPA/SBA-15	78
5-HPA/P25	83
HPA/SiO_2	109
10-HPA/P25	112
15-HPA/P25	121
HPA/Al_2O_3	145
HPA/P25	187
30-HPA/P25	183
HPA/NP-TiO_2	214

In the same way, at the same loading (20%) titanium dioxide nanoparticles generates more acid sites in comparison with Degussa P25. Although both materials present the same composition, the crystallographic phases and even the surface area is different (62 m^2 g^{-1} for HPA/NP-TiO_2 and 39 m^2 g^{-1} for HPA/P25). This fact could be associated with the surface area can even change the distribution, coverage, and density of the acid sites in the catalyst. Then, materials with low surface area will exhibit a high density of the acid sites which opposite trend will have less density of the acid sites. On the other hand, HPA/SiO_2 and HPA/SBA-15 exhibited a difference of 31 µmol/g-cat which could be owning with the typical geometry and the surface area of both supports (19 vs 444 m^2/g, respectively). In general, the order of total acidity for the most relevant materials was the following: HPA/NP-TiO_2 > HPA/P25 > 30-HPA/P25 > HPA/Al_2O_3 > 15-HPA/P25 > 10-HPA/P25 > HPA/SiO_2 > HPA/SBA-15.

3.2. Catalytic activity

3.2.1. Screening of heterogeneous catalysts

All synthetized materials were evaluated in the catalytic condensation of limonene with benzaldehyde for obtaining 3-oxabyciclo[3.3.1] nonane. Table 4 shows the results obtained for each HPA supported material. After 5 h, total conversion was achieved for the homogeneous HPA and HPA supported on silica, nevertheless for these cases, selectivity to the desired target was 80 and 70%, respectively. For HPA supported on different morphologies of the TiO_2, a different behavior was observed. At 5 h, conversion of limonene decreased in the following order: HPA/P25 > HPA/NP-TiO_2. Typical distribution of the acid sites could be responsible of this behavior (specially, distribution of Brønsted acid sites). When density of the acid sites (defined as number of acid sites

Table 4
Catalytic activity of the HPA supported catalysts.

Catalyst	$-r_0$ (mmol g_{cat}^{-1} min^{-1})	Conversion of limonene after 5 h (%)	Selectivity to oxabicyclo [3.3.0] nonane*	TON** (mol/mol)
HPA	0.4	> 99	80	165
HPA/SiO_2	3.6	> 99	70	165
HPA/P25	2.6	92	72	153
HPA/NP-TiO_2	0.3	40	50	67
HPA/SBA-15	2.0	91	60	152
HPA/Al_2O_3	0.0	3	-	5

Reaction conditions: 50 °C, CH_2Cl_2 as solvent, 750 rpm. *Selectivity at 20% of conversion. Average rate and calculated as $-r_0 = (n_0-n_t)/t.m_{cat}$ where n_0 are the initial mole, n_t the moles at the time t, and m_{cat} is the mass of catalyst. **TON was calculated as mmol of limonene converted over mmol of HPA used in the synthesis.

divided by surface area) of these catalysts was compared, it was possible to stablish that the same order of density of acid sites (e.g., 3.45 μmol m^{-2} for HPA/NP-TiO_2 vs 4.80 μmol m^{-2} for HPA/P25) was achieved. Then, density of the acid sites could be crucial for conversion of limonene and further synthesis of 3-oxabyciclo[3.3.1] nonane as it has been reported previously for condensation of a well-known reaction of monoterpenes with aldehydes [50,51].

In addition, HPA dispersed on alumina did not achieve activity for this reaction. Although this material exhibited high acidity, the typical geometry (architecture) of each alumina could not favor the transformation of limonene with benzaldehyde. On the other hand, HPA appears to decompose on WO_3 phases at temperatures higher than 600 °C [52], however, our hypothesis points out to describe that either decomposition of HPA on these supports or the strength of the acid sites could be responsible for the non-catalytic activity in this reaction. Selectivity to 3-oxabyciclo[3.3.1]nonane at 20% of conversion was obtained in the next order: HPA > HPA/P25 > HPA/SiO_2 > HPA-SBA-15. As selectivity depends on the conversion of limonene in each heterogeneous catalyst, acidity and dispersion should be a critical factor for the synthesis of the desired target. Even though over silica, the excellent yield was achieved (TON = 165), this type of material has been reported previously [8] and it was tested for comparison. HPA over alumina only achieved 3% of conversion with a poor value of TON. Apparently, their type and strength of the acid sites are not appropriate to drive the condensation of limonene with benzaldehyde. In general, it appears that HPA/P-25 catalyst is an active and selective catalyst for this reaction.

Fig. 4 shows that the selectivity to 3-oxabyciclo[3.3.1]nonane and the conversion of limonene change over reaction time for the HPA supported catalysts. HPA supported on alumina, silica and titanium dioxide nanotubes were the less active materials. On the other hand, it is interesting to appreciate that HPA/SBA-15 displayed a 70% of conversion and a selectivity of 70% at 1 h of reaction. Nevertheless, when time increases, a decreasing of 3-oxabyciclo[3.3.1]nonane is observed. This fact is attributed to an increasing of isomerization side reaction, which occur typically in the strong acid sites of the material. Then, considering these results and for further experiments, HPA/P25 was chosen as heterogeneous catalyst. Although HPA/SiO_2 was also an active material, this catalyst was not chosen because have been reported previously [29] and in fact, would not give new insight into the perspective of our research. For this reason, this catalyst was only tested for comparison.

3.2.2. *Effect of reaction conditions*

To further evaluate different reaction conditions for the highly selective synthesis of 3-oxabyciclo[3.3.1] nonane, different amounts of benzaldehyde, the volume of solvent and temperature were evaluated directly in the conversion and selectivity to the desired target using

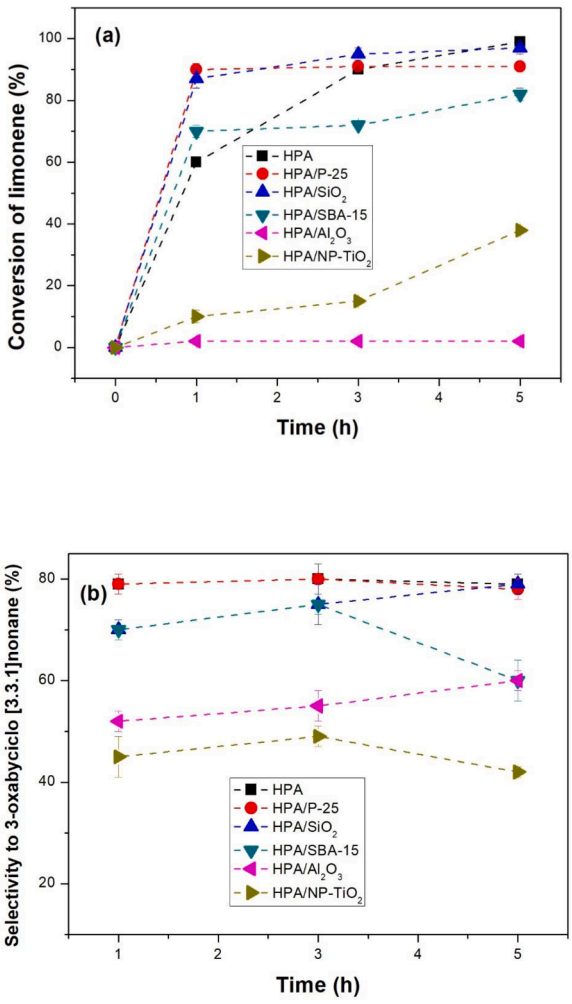

Fig. 4. Conversion of limonene (a) and selectivity to 3-oxabicyclo [3.3.1] nonane (b) using several HPA supported materials. Reaction conditions: 30 mg of catalyst, CH_2Cl_2 as the solvent, 750 rpm, 1 mmol of Limonene, 3 mmol of benzaldehyde. The dashed lines were included to guide the eyes.

HPA/P25 as heterogeneous catalyst. Fig. 5 (a) shows the effect of the excess of benzaldehyde within the conversion and selectivity. Interestingly when increases the amount of benzaldehyde, increases slightly conversion with time, however, no significant changes are observed. At 5 h of reaction, no differences in the conversion were seen when decreased the amount of benzaldehyde (from 2.9 to 2.0 mmol), nevertheless, a decrease to 92% was achieved with 3.6 mmol of the aldehyde. The same behavior was noted when the amount of aldehyde increased. With respect to selectivity, significant changes were observed when decreased the mmol of benzaldehyde at 1 h reaction while at 3 and 5 h no major differences were seen. When increased the time, selectivity to 3-oxabyciclo[3.3.1]nonane decreased slightly when 3.0 mmol of benzaldehyde was used. On the contrary, for 2.9 mmol of benzaldehyde selectivity to the desired target increased while that for 2.0 mmol remained constant. It seems that the optimum amount of benzaldehyde to obtain a maximum yield to 3-oxabicyclo[3.3.1]nonane is 2.9 mmol which was the same amount used for the screening catalytic experiments. An excess of benzaldehyde (3.6 mmol) decreases the interaction of this molecule within the acid sites of the catalyst, and then limonene tends to isomerize decreasing the selectivity to the desired oxabicyclic target. Maybe activation of the aldehyde and coverage are not appropriate to the further nucleophilic attack of limonene in the C=O bond of benzaldehyde.

On the other hand, Fig. 5 (b) shows the effect of the solvent volume

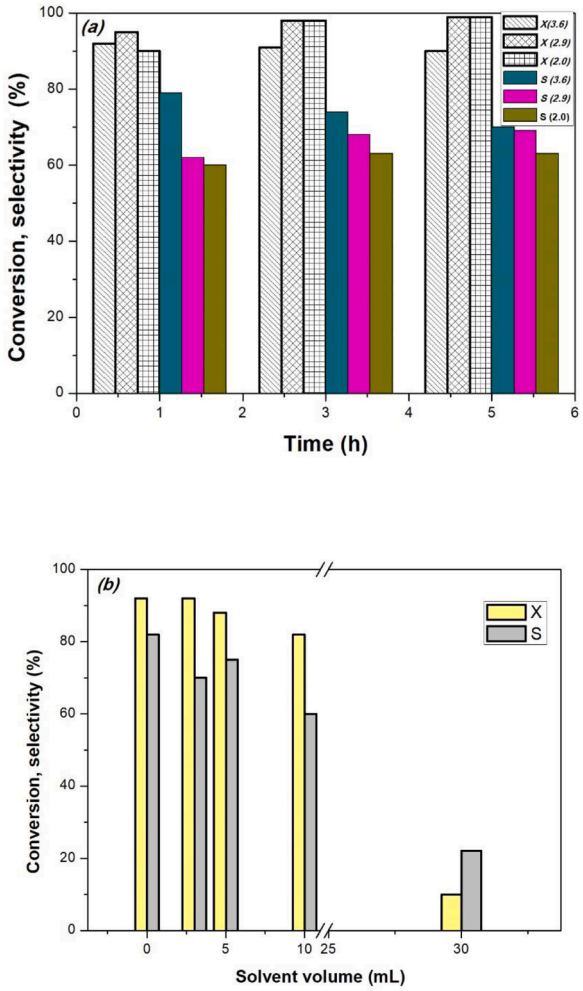

Fig. 5. Conversion of limonene and selectivity to 3-oxabicyclo[3.3.1]nonane with the variation of benzaldehyde (a) and with different volume of solvent (b). X = Conversion, S = Selectivity. Reaction conditions: 30 mg of catalyst (HPA/P25), CH2Cl2 as the solvent, 750 rpm, 1 mmol of Limonene, 3 mmol of benzaldehyde.

on the catalytic activity of HPA/P25. For solvent volume up to 5 mL conversion is not affected significantly, while selectivity decreased to 70%. A decrease in both conversion and selectivity is observed for a larger volume of solvents (e.g., 10 and 30 mL) which is due to the production of another product (side isomerization reaction) and to a competition of limonene within the active sites of the catalyst. As dichloromethane is a Lewis acid [53], with a larger amount of solvent it could react with limonene, generating a block of the active sites of the catalyst. An aspect to highlight is that when no solvent is used the maximum conversion and selectivity were reached in comparison to when a different volume of solvent was used. In addition, with a decrease in the initial concentration (when increases the solvent volume), the condensation rate will decrease and then the contribution of isomerization will increase. This hypothesis is in line with the experimental results obtained in this research.

Considering the insight obtained previously, the effect of temperature was also explored in the catalytic conversion of limonene with benzaldehyde over HPA/P25. For this, two temperatures were used for further comparison (298 and 323 K, Fig. 6); it seems that at 323 K, the maximum conversion is achieved at only 1 h while that at room temperature and at 5 h, conversion of around 80% is achieved. However, selectivity to the desired 3-oxabicyclico[3.3.1] nonane decreased as temperature decreased. At room temperature, the major products are isomers of limonene while at 323 K the major product is 3-oxabicyclico [3.3.1] nonane. A possible reason for this fact could be associated with the activation of the benzaldehyde during its interaction with the acid sites of the catalyst. In general, temperature appears to affect some of the kinetics for different condensation reactions becoming more active when temperature increases [54,55]. Further investigations about how temperature affects the kinetics performance of this reaction are currently in progress.

3.2.3. *Effect of the HPA loading over P25*

It has been reported that HPA loading affects drastically the catalytic efficiency of HPA/P25 and the acid sites (Section 3.1.7). In this research, this effect was evaluated in the condensation of limonene with benzaldehyde for further synthesis of 3-oxabicyclico[3.3.1] nonane. Considering this aspect, in this research the effect of HPA loading over P25 was evaluated in a range of 5 up to 30% and the results are indicated in Fig. 7. With loading up to 10% no conversion and selectivity were obtained while when increases the amount of HPA on P25 (from 15% to 30%) both conversion and selectivity are increased. It is seeming that the optimum amount of HPA which further obtains the desired selectivity to 3-oxabyciclo[3.3.1] nonane and conversion of limonene is 20% wt. No significant differences in conversion nor selectivity were achieved when HPA loading was 25% and 30%, respectively. Differences in the catalytic activity for loadings below of 15% could be associated to two factors: (1) a deficiency in the coverage of HPA over P25 and (2) the

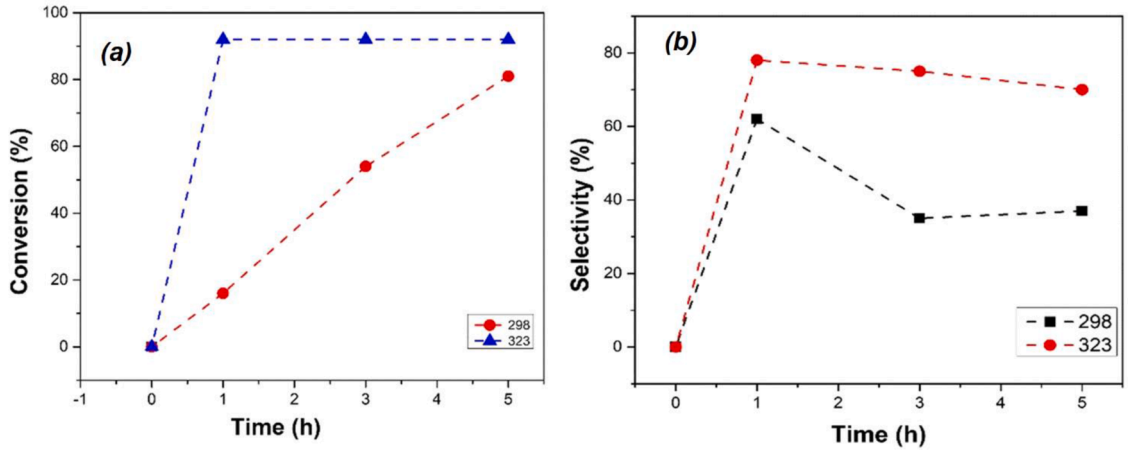

Fig. 6. Effect of temperature in the conversion of limonene (a) and selectivity to 3-oxabicyclo [3.3.1]nonane (b) at different times. Reaction conditions: 30 mg of catalyst, CH2Cl2 as the solvent, 750 rpm, 1 mmol of limonene, 3 mmol of benzaldehyde.

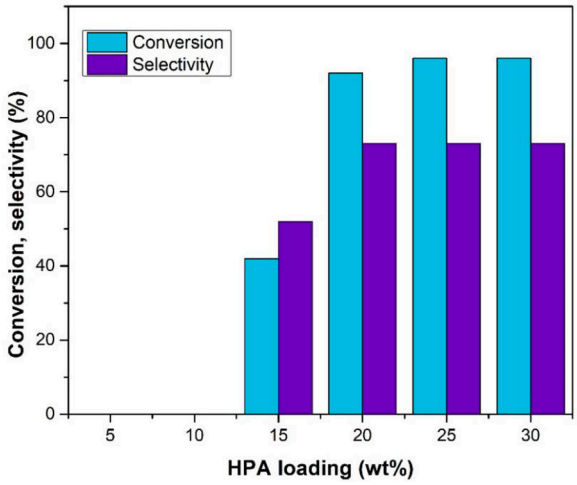

Fig. 7. Effect of HPA loading over P25 in the conversion of limonene and selectivity to oxabicycle [3.3.0]nonane at 5 h. Reaction conditions: 30 mg of catalyst, CH2Cl2 as the solvent, 750 rpm, 1 mmol of limonene, 3 mmol of benzaldehyde.

amount and density of acid sites quantified in the surface of P25. Although even with 25 and 30% wt a slight increase of conversion was achieved, the value of TON decreased and then the sustainability of the process seems to be affected.

3.2.4. Catalytic condensation with essential oils and a mixture of monoterpenes/sesquiterpenes

To further evaluate the catalytic potential of HPA/P25 in the selective synthesis of 3-oxabyciclo[3.3.1]nonane, even, in complex mixtures (see Table S1 in the supporting information), different additional reactions were evaluated at the same conditions that for catalytic condensation of benzaldehyde with limonene. Fig. 8 shows the weight composition of two essential oils: *Rosmarinus* and *orange* essential oils at the beginning and after the reaction with benzaldehyde and HPA/P25. In the case of *Rosmarinus* essential oil, it seems that the initial composition has different monoterpenes which include α-pinene (19%), β-pinene (12%), camphene (8%), *p*-cymene (4%), limonene (16%) among other (such as terpinolene, terpinene, etc which their sum is 41%). After condensation with benzaldehyde and the HPA/P25 catalyst, the composition varies significantly, giving 3-oxabicyclico[3.3.1] nonane as the major product (up to 25%), with a different composition of monoterpene (α-pinene: 13%, p-cymene:7%, limonene 4%, other 47%). An increased in the amount of p-cymene is attributed to dehydration products on the acid sites of the material as well as to the isomerization of α-pinene, β-pinene and limonene (which decreased significantly after catalytic condensation).

In the case of orange essential oil, which contains as major product limonene (92%), their composition varies in a range of monoterpenes such as α-pinene (0.5%), sabinene (2%), myrcene (0.5%) and other (5%, with similar molecular weight). In this research, after condensation with benzaldehyde, the large amount of limonene is transformed into 3-oxabicyclico[3.3.1] nonane changing significantly the composition of the essential oil. These results are like that obtained with limonene reactant grade because of their similar purity. Differences in both cases are attributed to impurities in the samples. On the other hand, these results also show that, even, in crude biomass such as essential oils, the reaction between limonene and benzaldehyde appears to carry out successfully with the HPA/P25 catalyst.

3.2.5. Laboratory scaling up

Because of the excellent yield and behavior of the HPA/P25 catalyst, the synthesis of the desired target was evaluated at different laboratory scales and the results are shown in Fig. 9. It is possible to see that regardless of the amount of catalyst, the same conversion and selectivity are achieved showing that this process is highly robust and sustainable at the conditions evaluated. Considering this fact, further configuration of the process to carry out continuously is shown in Fig. S4 (in the

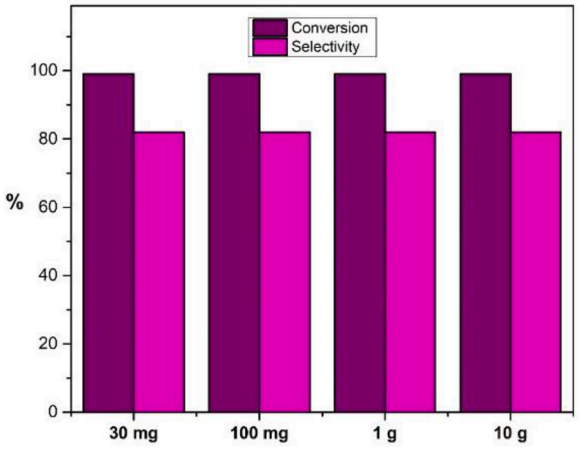

Fig. 9. Laboratory scaling up of the synthesis of 3-oxabyciclo[3.3.1]nonane from limonene and benzaldehyde with different amounts of HPA/P25. Reaction conditions: 50 °C, solvent-free, 750 rpm,.

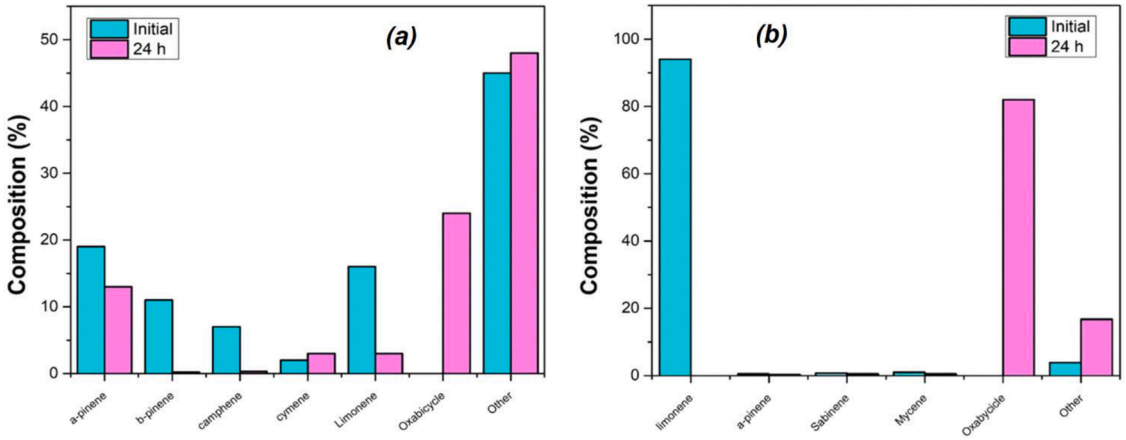

Fig. 8. Initial and final (24 h) compositions of Rosmarinus (a) and orange essential oils (b) with the catalytic condensation with benzaldehyde and HPA/P25 catalyst. Reaction conditions: 30 mg of catalyst, CH_2Cl_2 as the solvent, 750 rpm, 50 °C.

supporting information) using cinnamaldehyde as aldehyde for the condensation. This compound was chosen because of its fragrance properties. Besides, cinnamaldehyde can be extracted from natural sources, increasing the sustainability of the process. Further analysis for application in additives is currently performed in our laboratories.

3.2.6. Stability and reuse of the catalyst

The reuse of heterogeneous catalysts is an important parameter to evaluate in order to show the robustness of the material. In this way, HPA/P25 was removed from the suspension and reused again in another catalytic reaction. For this purpose, the catalyst was separated by using centrifugation and then washed twice with dichloromethane (x 2) and with ethyl acetate (x 1). Afterward, the catalyst was dried at room temperature, grinding at the particle size (for avoiding possible internal mass transfer limitation, Section 3.2.9.1) and reused under the same reaction conditions. Results are presented in Fig. 10 (a). As can be observed, both conversion of limonene and selectivity to 3-oxabicyclico [3.3.0] nonane remains constant until the second use of the catalyst. Then, both conversion and selectivity decreased to 70% and 30%, respectively. In the fourth use, the conversion of the limonene slightly decreased while selectivity decreased considerably (19%). In the third and fourth reuse, a high distribution of limonene isomers was obtained rather than 3-oxabyciclo[3.3.1]nonane.

When the lixiviation test was performed, Fig. 10 (b), the catalyst was removed (using hot filtration) from the solution for the first 5 min and left in constant stirring for another 55 min (up to 1 h). Although a slight increase in the conversion was observed (from 15% to 19%), selectivity to the desired was constant. In comparison when the catalyst was not removed from the medium, conversion increased obtaining the same catalytic activity that those reported in previous sections. In general, at 1 h of reaction and at the reaction conditions tested in this manuscript, no evident lixiviation was achieved. To further verify the reasons for the decreasing of both conversion and selectivity in the reaction of limonene and benzaldehyde, characterization by XRD, SEM, physisorption and TGA was carried out and analyzed elsewhere for the catalyst fresh and reused after its 3rd activity.

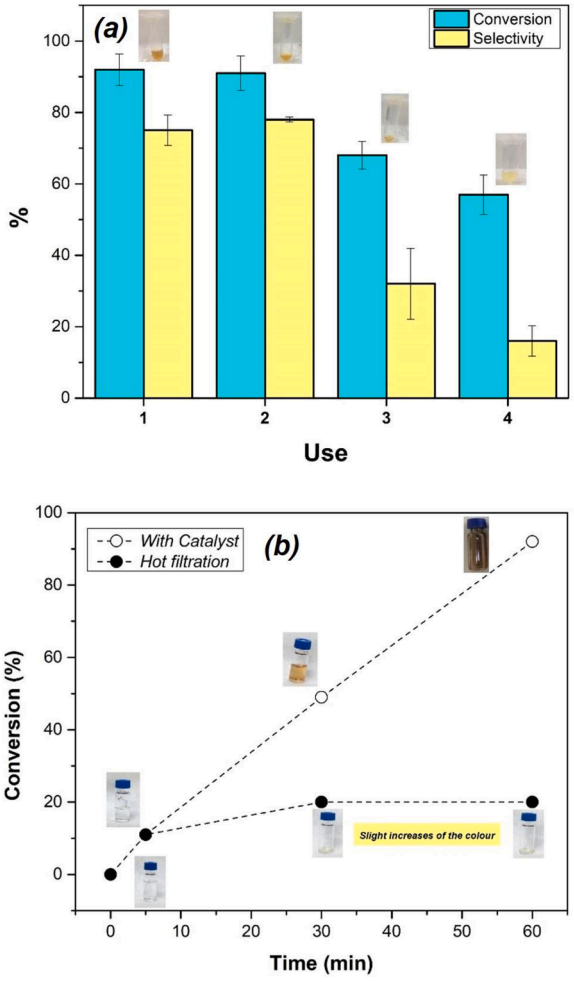

Fig. 10. Reuse of HPA/P25 on the selective synthesis of 3-oxabyciclo[3.3.1] nonane (a). Lixiviation test (b). Reaction conditions: 200 mg of catalyst, 1 mmol of limonene, 3 mmol of benzaldehyde, 50 °C, 750 rpm, 24 h. Experiments were performed by triplicated.

Fig. S5 (in the supporting information) shows the XRD pattern of HPA/P25 catalyst after different reuses. As can be seen typical structure of titanium dioxide (anatase phase) do not change after reuse of the material, however intensity decreased in some of the planes (2θ = 25°,48°,63° and 75°). But, in general, it appears that typical crystalline structure of the material does not change significantly. Even, when SEM micrographs were taken (Fig. S6 in the supporting information) in both fresh and reused catalyst, it seems that no changes in the typical morphology are observed.

Considering the feature that neither morphology and crystallographic structure did not change after reuse of the material, thermogravimetric analysis was performed, and the results are showed in Fig. 11. As can be seen two different events are well stablished, the first one at temperatures lower than 100 °C and another between 200 and 400 °C. The first one is well stablished to be associated with physiosorbed water while the second should correspond to organic species on the catalyst. This difference is well significative in the reused and fresh materials. It can be observed that for fresh catalyst no thermic events after 200 °C were seen, while that for the reused materials, clear events for temperatures between 200 and 400 °C related with adsorption of organic compounds is evident. After calculations, TG analysis showed a loss of mass because of the organic compounds at around 2–3% which could explain why catalyst loss activity after its second reuse. Another reason of the loss of activity could be also associated with the loss of acid sites during the performance of reaction. To further studies we are trying to study this phenomenon using *in-situ* and in operando equipment.

3.3. Kinetic assessments

3.3.1. Internal mass transfer limitation

Internal mass transfer limitations can be evaluated by the analysis of the reaction at different particle sizes and through the calculation of the Weisz-Prater criterion (CWP), Eq. (1). This parameter is used to check whether the reaction is limited or not by internal diffusion [56]. Experimentally, different aliquots can be taken from the reaction medium (at the same reaction conditions, particularly at different particle

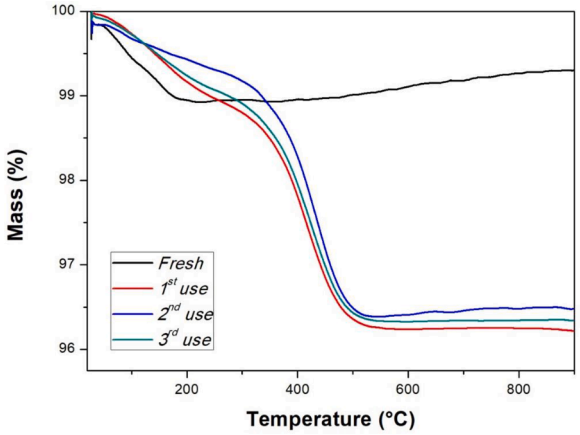

Fig. 11. Thermographs of fresh and reused HPA/P25.

sizes or at the same particle size and varying the initial concentrations of the reactants) and then reaction rate can be obtained. If CWP is <<1 the internal diffusion is negligible. However, a more precise criterion is CWP≤ 3*b*, where b is the maximum decrease in concentration gradient in pores, which is a function of the reaction order. The *b* values of 0.1, 0.2 and 2 are estimated for the second, first and zero-order reaction, respectively [57]. In this research, the reaction order is closer to 1.0 (see a comparison in Fig. S7 in the supporting information), then the values of CWP must be lower than 0.6.

$$CWP = \frac{-r_{A0}\rho_{cat}{R_{cat}}^2}{D_{AB}C_{A,cat}} \quad (1)$$

Where r_{A0} is the limonene (A) initial reaction rate, ρ_{cat} is the solid catalyst density, R_{cat} is the average radius of the catalyst particle (taken as an average of the particle size given for the mesh), D_{AB} is the effective diffusivity of limonene into benzaldehyde (B) at 323 K, and $C_{A,cat}$ is the concentration of limonene at the catalyst surface.

Diffusion coefficient can be calculated using the Wilke-Chang Eq. (2):

$$D_{AB} = \frac{1.173x10^{-16}(\varnothing M_B)^{\frac{1}{2}}T}{\mu_S {V_S}^{0.6}}\left(\frac{\varphi\sigma}{\tau}\right) \quad (2)$$

Where μ_S is the viscosity of the solution (0.001321 kg s^{-1} m^{-1}), V_S is the molar volume of the solvent at the normal boiling point (or at least of the fluid where is dissolving the limiting reactant; 0.01 m^3 $kmol^{-1}$), $\varnothing$ is the association parameter of benzaldehyde (2.26), M_B is the molecular weight of benzaldehyde (112.16 kg $kmol^{-1}$) and T is the absolute temperature (323 K), φ is the catalyst porosity (0.01), σ is the constriction factor (0.8) and τ is the tortuosity (3) [58]. Typical data of viscosity, molar volume and association parameters were obtained using Aspen Plus software. Table 5 shows the values of the Weisz-Prater criterion (CWP) obtained after evaluating different particles sizes, and it is seeming that no internal mass transfer is presented at the particle sizes tested in this research (the limit for avoiding internal mass transfer using the Weisz-Prater criterion (CWP) is 0.6). Then, for further kinetic studies, the catalyst was ground between 45 and 25 μm and tested in the reaction.

3.3.2. Kinetic modeling

The kinetic analysis of the condensation of limonene with benzaldehyde, (Eq. (3)), was done with experimental data at several reaction conditions collected from the liquid-phase solvent-free batch reaction; C is the main target of the reaction -3-oxabyciclo[3.3.1]nonane- and D, are the by-products obtained by the isomerization reaction of limonene over the acid sites of heteropoly acid material. The reaction rates calculated by the initial reaction rate method in the different tests are compared with proposed kinetic models.

$$\mathbf{A + B \rightarrow C + D} \quad (3)$$

To establish accurate kinetic models, all the data was collected under the absence of internal mass transfer limitations. The absence of external mass transfer limitations is guaranteed at high stirring rate of around 750 rpm according with our preliminary studies involving similar monoterpenes. The kinetic parameters obtained through an optimization of the sum of squared errors in the objective function *OF* in Eq. (4) fitting calculations of the experimental initial reaction rate $r'_{A0,exp}$ with some kinetics expressions r'_{A0} are indicated in Table 6. The minimization of the *OF* was carried out incorporating the Genetic Algorithm in Matlab software. Additionally, some stats parameters such as the coefficient of determinations (R^2 and R^2_{adj}), variance s^2, root mean square deviation R_{mds} and the 95% confidence interval CI_{95} included in Table 6 discriminate between the different models proposed.

$$OF = \sum \left(r'_{A0,exp} - r'_{A0}\right)^2 \quad (4)$$

The suggested kinetics expressions analyzed in this study were stablished from heterogeneous reaction theory based on the Langmuir-Hinshelwood-Hougen-Watson (LHHW) and Eley-Rideal (ER) mechanisms, along with a power law based pseudo-homogeneous (pH) model.

Pseudo-Homogeneous Irreversible Model (pH)

A homogeneous-like model was tested using the experimental data, for the purpose of evaluating a possible simplification of the heterogeneous kinetics adapted to the homogeneous model. From the results shown Table 4 can be concluded that it appears that the reaction rate has a higher dependence on the limonene concentration than the benzaldehyde due to the values obtained for the parameters α and β. A good adjustment ($R^2 = 0.9897$) was found with values of almost 0.4 and 0.05 for the reaction orders of limonene and benzaldehyde, respectively. Then, kinetics is government mainly for the concentration of limonene in the solution instead of the concentration of benzaldehyde. Considering these aspects as well as that the reaction is experimentally catalyzed by a heterogeneous system, the ER and LHHW models were further taken into consideration.

Heterogeneous Eley-Rideal (ER) Model

A heterogeneous kinetic model was tested based on the Eley-Rideal theory. In this type of reaction mechanism requires that only one of the two reactants be adsorbed on the surface of the catalyst. Here we fitted the experimental data of the initial reaction rate of limonene against the kinetic model obtained considering:

- Only adsorption of limonene on the surface of the catalyst (A + S = A.S).
- The reaction of the adsorbed specie A.S with benzaldehyde assumed as the limiting step to obtain (adsorbed or not) the main product 3-oxabyciclo[3.3.1] nonane (A.S + B → C + S or A.S + B → C.S).
- The kinetic may not depend, i.e., C_B almost constant, (ER-I) or may depend (ER-II) on the concentration of benzaldehyde according with the low β parameter obtained from pH model.

The kinetic expression obtained from previous considerations and evaluated at the initial conditions due to the implementation of the initial reaction rate method, lead to the kinetic models ER-I and ER-II shown in Table 4. The best adjustment ($R^2 = 0.9901$) of the experimental data was found from the kinetic model ER-I with a similar value of the kinetic constant k_1 obtained for both pH and ER-I models and the highest adjusted coefficient of determination ($R^2_{adj} = 0.9876$) between all models. This model supports the idea that the kinetic of this reaction is government mainly by the concentration of limonene in the solution instead of the concentration of benzaldehyde which is considered almost constant, adding to this narrative the suggestion of a contribution due to the adsorption of limonene on the surface of the material. The evaluation of the model considering the effect of the concentration of benzaldehyde was analyzed by the ER-II model which gave the lowest adjusted coefficient of determination ($R^2_{adj} = 0.8666$) ant the highest root means square deviation ($R_{msd} = 4.1573 \times 10^{-11}$).

Langmuir-Hinshelwood-Hougen Watson (LHHW) Model

On the other hand, another typical heterogeneous kinetic model based on the Langmuir-Hinshelwood-Hougen-Watson theory was considered for fitting the reaction data. This model requires that both reactants be adsorbed on the surface of the catalyst. Here we fitted again the experimental data of the initial reaction rate of limonene against the mathematical model obtained considering:

Table 5
Weisz-Prater criterion for different particles size tested in this research.

Range of particle size (μm)	Average particle size (μm)	Weisz-Prater Criterion (CWP)
75 < dp < 100	88	0.022
45 < dp < 75	60	0.009
45 < dp < 25	35	0.002

Table 6
Mathematical values of each variable in the kinetic modeling.

Model	*Rate law (mol g^{-1} min^{-1})*	*Constant*	*Value* ± *CI_{95}* **Value*	**CI_{95} x10^{-5}	*OF*x10^{6}	R^2 (R^2_{adj})	R_{msd} x10^{13}	s^2x10^{5}
pH	$-r'_{A0} = k_1 C_{A0}^{\alpha} C_{B0}^{\beta}$	k_1	0.11699	0.233	1.526	0.9897(0.9828)	3.8818	2.9596
		α	0.39587	1.391				
		β	0.05478	1.460				
ER-1	$-r'_{A0} = \frac{k_1 C_{A0}}{1 + K_1 C_{A0}}$	k_1	0.12073	0.1084	1.4653	0.9901(0.9876)	3.5786	2.95958
		K_1	0.20503	0.2428				
ER-1I	$-r'_{A0} = \frac{k_1 C_{A0} C_{B0}}{1 + K_1 C_{A0}}$	k_1	0.01614	0.0865	1.4653	0.8933(0.8666)	415.76	2.95958
		K_1	1.87485	10.34				
LHHW-I	$-r'_{A0} = \frac{k_1 C_{A0}}{(1 + K_1 C_{A0} + K_2)^2}$	k_1	0.38546	1391	1.554	0.9895(0.9825)	4.0272	2.95958
		K_1	0.10695	386				
		K_2	0.91779	6920				
LHHW-II	$-r'_{A0} = \frac{k_1 C_{A0} C_{B0}}{(1 + K_1 C_{A0} + K_2 C_{B0})^2}$	k_1	0.07335	0.0023	1.2618	0.9915(0.9858)	2.6537	2.95958
		K_1	0.22131	0.0630				
		K_2	0.13723	0.0169				

*Simulation conditions by the GA (population size: 300, generations: 10,000, OF and parameters tolerance = 1 × 10−8). ** CI95 calculated by coupling the GA to a nonlinear least-squares regression function (nlinfit) using optimal GA values outputs as inputs (tolerance = 1 × 10−8). k1 = pseudo-kinetic constant, K1, K2 = Adsorption constants, α and β reaction order.

- A possible both adsorption of limonene on the surface of the catalyst (A + S = A.S) and the adsorption of benzaldehyde as well (B + S = B.S).
- The reaction of the adsorbed species A.S and B.S is assumed as the limiting step to obtain (adsorbed or not) the main product 3-oxabyciclo[3.3.1] nonane (A.S + B.S → C + 2S or A.S + B.S → C.S + S).
- The kinetic may not depend, i.e., C_B almost constant, (LHHW-I) or may depend (LHHW-II) on the concentration of benzaldehyde as in the analysis for ER model.

The parameters obtained from the kinetic expressions LHHW-I and LHHW-II evaluated at the initial conditions are shown in Table 6. Although the adjusted coefficient of determination of LHHW models were as good as the obtained from the ER-I, considering in this case C_B almost constant for LHHW-I model, results in an uncertain estimation of the 95% confidence interval CI_{95} for all kinetic parameters and the highest OF value. The lowest OF (1.2618×10^{-6}) and root mean square deviation ($R_{msd} = 2.6537 \times 10^{-13}$) value were obtained from the LHHW-II model which considers the contribution effect of the concentration of benzaldehyde in the kinetic expression. This new perspective of the reaction from LHHW-II model also seems in agreement with the assumption of adsorption of limonene on the surface of the catalyst, in this case higher than a possible adsorption of benzaldehyde because of the lower value of K_2 obtained compared with K_1.

4. Conclusions

Several heterogeneous catalysts of heteropolyacids supported on SBA-15, SiO_2, TiO_2 (Degussa P25, Al_2O_3, NP-TiO_2, were tested in the catalytic condensation of limonene with benzaldehyde. The synthesized materials were widely characterized giving insights into the way as heteropolyacids with a typical Keggin-like anion can be modified by the preparation methodology. XRD and physisorption evidenced a decrease of the surface area after HPA impregnation and besides that, this can be well dispersed. Similarly, ^{31}P NMR showed that apparently structure can be whether like α- $[PW_{12}O_{4O}]^{3-}$ or such as well dispersed decomposed HPA compound. Acidity by TPD- ammonia showed that almost all materials presented high content of acid sites and that evidently when increases the amount of HPA in TiO_2-P25, acidity increased until it was constant. Good to excellent yields towards the formation of 3-oxabyciclo [3.3.1]nonane at benign reaction conditions (50 °C, free solvent, 1 h) were achieved. The most promissory catalyst was HPA supported on titanium dioxide (Degussa P25) because of its textural and acidic properties (up to 187 μmol. $gcat^{-1}$). The reaction can be performed without solvent and under relatively soft conditions. Changes in the temperature can affect the yields towards the formation of the desired target. It was observed that a decrease until room temperature increases the formation of isomers byproducts giving a change of the distribution products and decreasing the synthesis of the desired 3-oxabyciclo[3.3.1] nonane. In addition, the effect of the reaction conditions was evaluated to establish whether solvent volume and time affect the performance of the reaction in course. It appears that an increase in the volume of the solvent decreases the amount of the desired target, giving high selectivity to isomers of limonene.

The effect of HPA loading on TiO_2-P25 was also explored, concluding that 20 wt% of HPA is enough to obtain the desired conversion and selectivity to 3-oxabyciclo[3.3.1]nonane. With the aim to increase the sustainability of the reaction, essential oils (*Rosmarinus* and orange oils), extracted directly from biomass with limonene as one of the components, were also tested obtaining different compositions where 3-oxabyciclo[3.3.1]nonane is the major component. Evidently, this showed that our catalyst (HPA/P-25) is selective, even, in samples of biomass.

Kinetic analysis suggests a typical LHHW mechanism, within the adsorption as a critical stage. Finally, the laboratory scaled-up of the reaction (up to 10 g) can be performed obtaining the same yields that when only 10 mg of sample was used. HPA/P25 is a heterogeneous catalyst robust since can be used several times with a slight decrease in the catalytic activity. This loss of activity was associated with fewer acid sites and with the adsorption of organic species on the surface of the material.

CRediT authorship contribution statement

Julián E. Sánchez-Velandia: Conceptualization, Data curation, Formal analysis, Investigation, Methodology, Validation, Visualization, Writing – original draft, Writing – review & editing. **Herme G. Baldoví:** Formal analysis, Methodology, Resources, Writing – review & editing. **A. Yu Sidorenko:** Formal analysis, Methodology, Writing – review & editing. **Jaime A. Becerra:** Conceptualization, Data curation, Formal analysis, Investigation, Methodology, Validation, Visualization, Writing – review & editing. **Fernando Martínez O:** Formal analysis, Funding acquisition, Project administration, Resources, Supervision, Writing – review & editing.

Declaration of Competing Interest

The authors declare the following financial interests/personal relationships which may be considered as potential competing interests: Julian E Sanchez Velandia reports financial support was provided by Colombia Ministry of Science Technology and Innovation. Julian E.

Sanchez Velandia reports financial support was provided by Colombian Ministry of Commerce Industry and Tourism. Julian E Sanchez Velandia reports financial support was provided by Industrial University of Santander. Jaime A Becerra Chala reports financial support was provided by Colombia Ministry of Science Technology and Innovation.

Data availability

Data will be made available on request.

Acknowledgments

This research was supported by Ministerio de Ciencia, Tecnología e Innovación, Ministerio de Educación Nacional; Ministerio de Industria, Comercio y Turismo, and ICETEX of Colombia through Programme Ecosistema Científico-Colombia Científica from Fondo Francisco José de Caldas, Colombia; Grant RC-FP44842-212-2018. J.S.V is grateful to Universidad Industrial de Santander, Colombia for his postdoctoral fellowship: "Apoyo Estancias Postdoctorales", 2020. J.A.B acknowledges Minciencias (before Colciencias), call 694, 2014.

Supplementary materials

Supplementary material associated with this article can be found, in the online version, at doi:10.1016/j.mcat.2022.112511.

References

[1] K.N. Mahmud, Z.A. Zakaria, Pyrolytic products from oil palm biomass and its potential applications, valroization of Agro-industrial residues- volume II: non-biological approaches. Applied Environmentl Science and Engineering for a Sustainable Future, Springer, 2020.
[2] M. Golets, S. Ajaikumar, J.P. Mikkola, Catalytic upgrading of extractives to chemicals: monoterpenes to "eXICALS, Chem. Rev. 115 (2015) 3141–3169, https://doi.org/10.1021/cr500407m.
[3] M.J. Climent, A. Corma, S. Iborra, Heterogeneous catalysts for the one-pot synthesis of chemicals and fine chemicals, Chem. Rev. 111 (2011) 1072–1133, https://doi.org/10.1021/cr1002084.
[4] N.F. Salakhutdinov, K.P. Volcho, O.I. Yarovaya, Monoterpenes as a renewable source of biologically active compounds, Pure Appl. Chem. 89 (2017) 1105–1117, https://doi.org/10.1515/pac-2017-0109.
[5] J.E. Sánchez-Velandia, J.F. Gelves, M.A. Márquez, L. Dorkis, A.L. Villa, Catalytic isomerization of α-pinene epoxide over a natural zeolite, Catal. Lett. (2020), https://doi.org/10.1007/s10562-020-03225-9.
[6] N.D. Shcherban, R.Y. Barakov, P. Mäki-Arvela, S.A. Sergiienko, I. Bezverkhyy, K. Eränen, D.Y. Murzin, Isomerization of α-pinene oxide over ZSM-5 based micro-mesoporous materials, Appl. Catal. A Gen. 560 (2018) 236–247, https://doi.org/10.1016/j.apcata.2018.05.007.
[7] Y. Noma, Y. Asakawa, Biotransformation of monoterpenoids. Comprehensive Natural Products II Chemistry and Biology 3, Elsevier, 2010, pp. 669–801, https://doi.org/10.1016/b978-008045382-8.00742-5.
[8] R.F. Cotta, K.A. da Silva Rocha, E.F. Kozhevnikova, I.V. Kozhevnikov, E. V. Gusevskaya, Heteropoly acid catalysts in upgrading of biorenewables: cycloaddition of aldehydes to monoterpenes in green solvents, Appl. Catal. B Environ. 217 (2017) 92–99, https://doi.org/10.1016/j.apcatb.2017.05.055.
[9] H. Martinez Q, Á.A. Amaya, E.A. Paez-mozo, F. Martinez O, S. Valange, Photo-assisted O-atom transfer to monoterpenes with molecular oxygen and a dioxoMo (VI) complex immobilized on TiO_2 nanotubes, Catal. Today (2020) 1–17, https://doi.org/10.1016/j.cattod.2020.07.053.
[10] C. Member, R.A.S.A.V. Kutchin, I.Y. Chukicheva, I.V Fedorova, O.A. Shumova, Alkylation of aluminum phenolate with unsaturated monoterpenes, 437 (2011) 776–777. 10.1134/S0012500811040124.
[11] M.J. Van Der Werf, K.M. Overkamp, J.A.M. De Bont, Limonene-1,2-epoxide hydrolase from Rhodococcus erythropolis DCL14 belongs to a novel class of epoxide hydrolases, J. Bacteriol. 180 (1998) 5052–5057, https://doi.org/10.1128/jb.180.19.5052-5057.1998.
[12] M.B. Kolicheski, L.C. Cocco, D.A. Mitchell, M. Kaminski, Synthesis of myrcene by pyrolysis of β-pinene: analysis of decomposition reactions, J. Anal. Appl. Pyrolysis 80 (2007) 92–100, https://doi.org/10.1016/j.jaap.2007.01.005.
[13] A.Y. Sidorenko, Y.M. Kurban, I.V. Il'ina, N.S. Li-Zhulanov, D.V. Korchagina, O. V. Ardashov, J. Wärnå, K.P. Volcho, N.F. Salakhutdinov, D.Y. Murzin, V. E. Agabekov, Catalytic synthesis of terpenoid-derived hexahydro-2H-chromenes with analgesic activity over halloysite nanotubes, Appl. Catal. A Gen. (2021) 618, https://doi.org/10.1016/j.apcata.2021.118144.
[14] G. Baishya, B. Sarmah, N. Hazarika, An environmentally benign synthesis of octahydro-2 H-chromen-4-ols via modified montmorillonite K10 catalyzed Prins cyclization reaction, Synlett 24 (2013) 1137–1141, https://doi.org/10.1055/s-0032-1316915.
[15] I.V Il, N.S. Dyrkheeva, A.L. Zakharenko, A.Y. Sidorenko, N.S. Li-zhulanov, D. V Korchagina, R. Chand, D.M. Ayine-tora, A.A. Chepanova, O.D. Zakharova, E. S. Ilina, J. Reynisson, A.A. Malakhova, S.P. Medvedev, S.M. Zakian, K.P. Volcho, N. F. Salakhutdinov, O.I. Lavrik, Design, synthesis, and biological investigation of novel classes of 3-carene-derived potent inhibitors of TDP1, Molecules 25 (15) (2020) 1–22, https://doi.org/10.3390/molecules25153496.
[16] A.Y. Sidorenko, Y.M. Kurban, A.V. Kravtsova, I.V. Il'ina, N.S. Li-Zhulanov, D. V. Korchagina, J.E. Sánchez-Velandia, A. Aho, K.P. Volcho, N.F. Salakhutdinov, D. Y. Murzin, V.E. Agabekov, Clays catalyzed cascade Prins and Prins-Friedel-Crafts reactions for synthesis of terpenoid-derived polycyclic compounds, Appl. Catal. A Gen. (2022) 629, https://doi.org/10.1016/j.apcata.2021.118395.
[17] O.S. Patrusheva, K.P. Volcho, N.F. Salakhutdinov, Synthesis of oxygen-containing heterocyclic compounds based on monoterpenoids, Russ. Chem. Rev. 87 (2018) 771–796, https://doi.org/10.1070/rcr4810.
[18] R.F. Cotta, R.A. Martins, K.A. da Silva Rocha, E.F. Kozhevnikova, I.V. Kozhevnikov, E.V. Gusevskaya, Coupling of phenylacetaldehyde and styrene oxide with biorenewable alkenes in eco-friendly solvents, Catal. Today 381 (2021) 254–260, https://doi.org/10.1016/j.cattod.2020.05.068.
[19] L.C.A. Barbosa, L.B. Nogueira, C.R.Á. Maltha, R.R. Teixeira, A.A. Silva, Synthesis and phytogrowth properties of oxabicyclic analogues related to helminthosporin, Molecules 14 (2009) 160–173, https://doi.org/10.3390/molecules14010160.
[20] S.V. Kumar, A. Yen, M. Lautens, P.J. Guiry, Catalytic asymmetric transformations of oxa- and azabicyclic alkenes, Chem. Soc. Rev. 50 (2021) 3013–3093.
[21] A.Y. Sidorenko, A.V Kravtsova, P. Mäki-arvela, A. Aho, T. Sandberg, I.V Il, N.S. Li-zhulanov, D.V Korchagina, K.P. Volcho, N.F. Salakhutdinov, D.Y. Murzin, Synthesis of isobenzofuran derivatives from renewable 2-carene over halloysite nanotubes, Mol. Catal. 490 (2020), 110974, https://doi.org/10.1016/j.mcat.2020.110974.
[22] Y. Liu, Y. Wu, M. Su, W. Liu, X. Li, F. Liu, Developing Brønsted–Lewis acids bifunctionalized ionic liquids based heteropolyacid hybrid as high-efficient solid acids in esterification and biomass conversion, J. Ind. Eng. Chem. 92 (2020) 200–209, https://doi.org/10.1016/j.jiec.2020.09.005.
[23] M.B. Colombo Migliorero, V. Palermo, G.P. Romanelli, P.G. Vázquez, New niobium heteropolyacid included in a silica/alumina matrix: application in selective sulfoxidation, Catal. Today (2020), https://doi.org/10.1016/j.cattod.2020.10.034.
[24] H. Zhang, J. Liu, C. Liu, T. Wang, W. Zhu, High dispersion of heteropolyacid nanoparticles on hydrothermally Cs-modified three-dimensionally ordered macroporous SiO_2 with excellent selectivity in methacrolein oxidation, Chin. J. Chem. Eng. 28 (2020) 2785–2791, https://doi.org/10.1016/j.cjche.2020.07.017.
[25] L. Pizzio, P. Vázquez, C. Cáceres, M. Blanco, Tungstophosphoric and molybdophosphoric acids supported on zirconia as esterification catalysts, Catal. Lett. 77 (2001) 233–239, https://doi.org/10.1023/A:1013218307792.
[26] E. Matijević. Fine Particles in Medicine and Pharmacy, Springer, New York, 2011, ISBN 978-1-4614-0379-1, https://doi.org/10.1007/978-1-4614-0379-1.
[27] V. Negro, G. Mancini, B. Ruggeri, D. Fino, Citrus waste as feedstock for bio-based products recovery: review on limonene case study and energy valorization, Bioresour. Technol. 214 (2016) 806–815, https://doi.org/10.1016/j.biortech.2016.05.006.
[28] J.D. Tibbetts, S.D. Bull, p-menthadienes as biorenewable feedstocks for a monoterpene-based biorefinery, Adv. Sustain. Syst. 5 (2021) 2000292, https://doi.org/10.1002/adsu.202000292 (1-13).
[29] R.F. Cotta, K.A. da Silva Rocha, E.F. Kozhevnikova, I.V. Kozhevnikov, E. V. Gusevskaya, Coupling of monoterpenic alkenes and alcohols with benzaldehyde catalyzed by silica-supported tungstophosphoric heteropoly acid, Catal. Today 289 (2017) 14–19, https://doi.org/10.1016/j.cattod.2016.07.021.
[30] T. Pinto, K. Szeto, N. Oueslati, N. Essayem, V. Dufaud, F. Lefebvre, Comparison of the acidity of heteropolyacids encapsulated in or impregnated on SBA-15, Oil Gas Sci. Technol. (2016) 71, https://doi.org/10.2516/ogst/2016005.
[31] G. Marcì, E. García-López, M. Bellardita, F. Parisi, C. Colbeau-Justin, S. Sorgues, L. F. Liotta, L. Palmisano, Keggin heteropolyacid H3PW12O40 supported on different oxides for catalytic and catalytic photo-assisted propene hydration, Phys. Chem. Chem. Phys. 15 (2013) 13329–13342, https://doi.org/10.1039/c3cp51142a.
[32] Q. Jin, F. Qu, J. Jiang, Y. Dong, W. Guo, H. Lin, A pH-sensitive controlled dual-drug release from meso-macroporous silica/multilayer-polyelectrolytes coated SBA-15 composites, J. Sol Gel Sci. Technol. 66 (2013) 466–471, https://doi.org/10.1007/s10971-013-3033-6.
[33] J.E. Sánchez-Velandia, E.A. Páez-Mozo, F. Martínez-Ortega, A kinetic study of the photoinduced oxo-transfer using a Mo complex anchored to TiO_2, Rev. Fac. Ing. Univ. Antioq. (2020) 83–93, https://doi.org/10.17533/udea.redin.20200477.
[34] K. Djebaili, Z. Mekhalif, A. Boumaza, A. Djelloul, XPS, FTIR,EDX,XRD analysis of Al_2O_3 scales grown on Pm2000 alloy, J. Spectrosc. (2015) 1–16, https://doi.org/10.1155/2015/868109, 2013.
[35] Z. Wang, L. Liu, Mesoporous silica supported phosphotungstic acid catalyst for glycerol dehydration to acrolein, Catal. Today 376 (2021) 55–64, https://doi.org/10.1016/j.cattod.2020.08.007.
[36] J.E. Sánchez-Velandia, E. Pájaro, A.L. Villa, F. Martínez-O, Selective synthesis of camphene from isomerization of α- and β-pinene over heterogeneous catalysts, Microporous Mesoporous Mater. 324 (2021), https://doi.org/10.1016/j.micromeso.2021.111273.
[37] J. Wang, J. Yu, X. Zhu, X.Z. Kong, Preparation of hollow TiO_2 nanoparticles through TiO_2 deposition on polystyrene latex particles and characterizations of their structure and photocatalytic activity, Nanoscale Res. Lett. 7 (2012) 1–8, https://doi.org/10.1186/1556-276X-7-646.
[38] N. Xu, Z. Liu, Y. Dong, T. Hong, L. Dang, W. Li, Controllable synthesis of mesoporous alumina with large surface area for high and fast fluoride removal,

ceramics international 42 (2016) 15253–15260, https://doi.org/10.1016/j.ceramint.2016.06.164.
[39] V.S. Marakatti, D. Mumbaraddi, G.V. Shanbhag, A.B. Halgeri, S.P. Maradur, Molybdenum oxide/γ-alumina: an efficient solid acid catalyst for the synthesis of nopol by Prins reaction, RSC Adv. 5 (2015) 93452–93462, https://doi.org/10.1039/c5ra12106j.
[40] H. Zhang, J. Liu, C. Liu, T. Wang, W. Zhu, High dispersion of heteropolyacid nanoparticles on hydrothermally Cs-modified three-dimensionally ordered macroporous SiO2 with excellent selectivity in methacrolein oxidation, Chin. J. Chem. Eng. 28 (2020) 2785–2791, https://doi.org/10.1016/j.cjche.2020.07.017.
[41] A. Micek-Ilnicka, N. Ogrodowicz, U. Filek, A. Kusior, The role of TiO_2 polymorphs as support for the Keggin-type tungstophosphoric heteropolyacid as catalysts for n-butanol dehydration, Catal. Today 380 (2021) 84–92, https://doi.org/10.1016/j.cattod.2021.04.021.
[42] A. Borodziński, M. Bonarowska, Relation between crystallite size and dispersion on supported metal catalysts, Langmuir 13 (1997) 5613–5620, https://doi.org/10.1021/la962103u.
[43] A. Popa, V. Sasca, D. Bajuk-Bogdanović, I. Holclajtner-Antunović, Acidic nickel salts of Keggin type heteropolyacids supported on SBA-15 mesoporous silica, J. Porous Mater. 23 (2016) 211–223, https://doi.org/10.1007/s10934-015-0072-0.
[44] P. Apopei, C. Catrinescu, C. Teodosiu, S. Royer, Mixed-phase TiO_2 photocatalysts: crystalline phase isolation and reconstruction, characterization and photocatalytic activity in the oxidation of 4-chlorophenol from aqueous effluents, Appl. Catal. B Environ. 160–161 (2014) 374–382, https://doi.org/10.1016/j.apcatb.2014.05.030.
[45] B. Viswanadham, P. Jhansi, K.V.R. Chary, H.B. Friedrich, S. Singh, Efficient solvent free knoevenagel condensation over vanadium containing heteropolyacid catalysts, Catal. Lett. 146 (2016) 364–372, https://doi.org/10.1007/s10562-015-1646-9.
[46] Y. Liu, B. Cheng, K.K. Wang, G.P. Ling, J. Cai, C.L. Song, G.R. Han, Study of Raman spectra for γ-Al_2O_3 models by using first-principles method, Solid State Commun. 178 (2014) 16–22, https://doi.org/10.1016/j.ssc.2013.09.030.
[47] B. Reif, S.E. Ashbrook, L. Emsley, M. Hong, Solid-state NMR spectroscopy, Nat. Rev. Methods Prim. 1 (2021), https://doi.org/10.1038/s43586-020-00002-1.
[48] I.V. Kozhevnikov, Catalysis by heteropoly acids and multicomponent polyoxometalates in liquid-phase reactions, Chem. Rev. 98 (1998) 171–198, https://doi.org/10.1021/cr960400y.
[49] R.I. Maksimovskaya, G.M. Maksimov, 31P NMR studies of hydrolytic conversions of 12-tungstophosphoric heteropolyacid, Coord. Chem. Rev. 385 (2019) 81–99, https://doi.org/10.1016/j.ccr.2019.01.014.
[50] A.Y. Sidorenko, Y.M. Kurban, A.V. Kravtsova, I.V. Il'ina, N.S. Li-Zhulanov, D. V. Korchagina, J.E. Sánchez-Velandia, A. Aho, K.P. Volcho, N.F. Salakhutdinov, D. Y. Murzin, V.E. Agabekov, Clays catalyzed cascade Prins and Prins-Friedel-Crafts reactions for synthesis of terpenoid-derived polycyclic compounds, Appl. Catal. A Gen. (2021), 118395, https://doi.org/10.1016/j.apcata.2021.118395.
[51] A.Y. Sidorenko, A.V Kravtsova, P. Mäki-arvela, A. Aho, T. Sandberg, I.V Il, N.S. Li-zhulanov, D.V Korchagina, K.P. Volcho, N.F. Salakhutdinov, D.Y. Murzin, Synthesis of isobenzofuran derivatives from renewable 2-carene over halloysite nanotubes, Mol. Catal. 490 (2020), 110974, https://doi.org/10.1016/j.mcat.2020.110974.
[52] S.R. Matkovic, L.E. Briand, M.Á. Bañares, Investigation of the thermal stability of phosphotungstic Wells-Dawson heteropoly-acid through *in situ* Raman spectroscopy, Mater. Res. Bull. 46 (2011) 1946–1948, https://doi.org/10.1016/j.materresbull.2011.07.015.
[53] I. Pietro Oliveri, G. MacCarrone, S. Di Bella, A lewis basicity scale in dichloromethane for amines and common nonprotogenic solvents using a zinc(II) Schiff-base complex as reference lewis acid, J. Org. Chem. 76 (2011) 8879–8884, https://doi.org/10.1021/jo2016218.
[54] S. Bhasker-Ranganath, M.S. Rahman, C. Zhao, F. Calaza, Z. Wu, Y. Xu, Elucidating the mechanism of ambient-temperature aldol condensation of acetaldehyde on ceria, ACS Catal. 11 (2021) 8621–8634, https://doi.org/10.1021/acscatal.1c01216.
[55] K. Dhahagani, J. Rajesh, R. Kannan, G. Rajagopal, Asymmetric Henry reaction of aldehydes catalyzed by recyclable an MCM-41 supported copper(II) salen complex, Tetrahedron Asymmetry 22 (2011) 857–865, https://doi.org/10.1016/j.tetasy.2011.04.020.
[56] S.A. Zavrazhnov, A.L. Esipovich, S.Y. Zlobin, A.S. Belousov, A.V. Vorotyntsev, Mechanism analysis and kinetic modelling of Cu NPs catalysed glycerol conversion into lactic acid, Catalysts 9 (2019) 1–6, https://doi.org/10.3390/catal9030231.
[57] D. Casas-Orozco, E. Alarcón, A.L. Villa, Kinetic study of the nopol synthesis by the Prins reaction over tin impregnated MCM-41 catalyst with ethyl acetate as solvent, Fuel 149 (2015) 130–137, https://doi.org/10.1016/j.fuel.2014.08.067.
[58] H. Fogler. Elements of Chemical Reaction Engineering, Prentice Hall, 2010.